# Downloaded from https://www.science.org at Columbia University on January 07, 2023

### **NEUROSCIENCE**

# Blood flows from the SCN toward the OVLT within a new brain vascular portal pathway

Ranjan K. Roy<sup>1,2</sup>, Yifan Yao<sup>3</sup>, Isabella K. Green<sup>3</sup>, Andrew V. Aitken<sup>4</sup>, Vinicia C. Biancardi<sup>4</sup>, Rae Silver<sup>3,5,6,7</sup>, Javier E. Stern<sup>1,2</sup>\*

The suprachiasmatic nucleus (SCN) sets the phase of oscillation throughout the brain and body. Anatomical evidence reveals a portal system linking the SCN and the organum vasculosum of the lamina terminalis (OVLT), begging the question of the direction of blood flow and the nature of diffusible signals that flow in this specialized vasculature. Using a combination of anatomical and in vivo two-photon imaging approaches, we unequivocally show that blood flows unidirectionally from the SCN to the OVLT, that blood flow rate displays daily oscillations with a higher rate at night than in the day, and that circulating vasopressin can access portal vessels. These findings highlight a previously unknown central nervous system communication pathway, which, like that of the pituitary portal system, could allow neurosecretions to reach nearby target sites in OVLT, avoiding dilution in the systemic blood. In both of these brain portal pathways, the target sites relay signals broadly to both the brain and the rest of the body.

Copyright © 2024 The Authors, some rights reserved; exclusive licensee American Association for the Advancement of Science. No claim to original U.S.
Government Works.
Distributed under a Creative Commons Attribution
NonCommercial
License 4.0 (CC BY-NC).

### INTRODUCTION

The portal pathway linking the capillary beds of the hypothalamus and pituitary was first described in 1933 and was long believed to be the only such vascular pathway in the brain (1). Almost 90 years later, that unique position changed with our discovery of a second portal pathway connecting the mouse suprachiasmatic nucleus (SCN), the circadian clock in the brain, and the organum vasculosum of the lamina terminalis (OVLT), a nearby circumventricular organ (CVO) (2). Portal pathways provide a mechanism whereby small populations of neurons can produce effective concentrations of secretions that reach their targets via a local vascular system, thereby avoiding dilution in the general circulatory system. The functional significance of this previously unknown neurovascular OVLT portal pathway (SCN-OVLTp) requires unveiling the direction of blood flow between these nuclei. This, in turn, will permit determination of the source and the target of signals traveling in this system and its functions. It is worth noting that, in the case of the hypothalamic-pituitary portal system, this nexus of studies regarding the direction of blood flow took about two decades (3), and many years thereafter led to the 1977 Nobel Prize in Physiology or Medicine to Guillemin and Schally.

A great deal has been written about the SCN, the OVLT, and CVOs. The SCN lies at the base of the brain, just above the optic chiasm, adjacent to the third ventricle. Neuronal efferents from the SCN reach numerous central nervous system targets (4–6) including the OVLT (7). However, it is also well-established that the SCN produces neurosecretions that exhibit daily rhythms (8–10) and that diffusible signals are sufficient to sustain circadian rhythms (11). Thus, when transplanted into the third ventricle, the grafted SCN,

<sup>1</sup>Neuroscience Institute, Georgia State University, Atlanta, GA, USA. <sup>2</sup>Center for Neuroinflammation and Cardiometabolic Diseases, Georgia State University, Atlanta, GA, USA. <sup>3</sup>Department of Psychology, Columbia University, New York, NY, USA. <sup>4</sup>Department of Anatomy, Physiology and Pharmacology, Auburn University, Auburn, AL, USA. <sup>5</sup>Department of Neuroscience and Behavior, Barnard College, New York, NY, USA. <sup>6</sup>Department of Pathology and Cell Biology Graduate Program, Columbia University, New York, NY, USA. <sup>7</sup>Zukerman Institute Affiliate, Columbia University, New York, NY, USA.

\*Corresponding author. Email: jstern@gsu.edu

even when placed within a capsule that prevents fiber outgrowth can restore locomotor, drinking and gnawing rhythms in animals in which this nucleus has been ablated [reviewed in (12–14)]. In addition, in an ex vivo slice preparation, SCN neuropeptides including vasoactive intestinal peptide (VIP), arginine vasopressin (AVP), and gastrin releasing peptide (GRP) secreted by a "donor" SCN can support rhythmicity in recipient arrhythmic SCN "host" tissue (15).

Like the SCN, the OVLT lies immediately above the optic chiasm near the anterior wall of the third ventricle. The OVLT is a sensory CVO bearing fenestrated capillaries and is enriched in receptors for hormones and neuropeptides (16, 17). The fenestrated capillaries allow systemic circulating factors to permeate into the brain parenchyma and the cerebrospinal fluid (CSF) and to reach the sensory neurons of the OVLT. Information can then be relayed from OVLT to numerous targets, including the supraoptic nucleus (SON), paraventricular nucleus, median preoptic nucleus, and the SCN itself (17, 18) via its neural efferents, and to the CSF via its leaky blood vessels. The OVLT is implicated in a variety of centrally regulated processes, many of which have daily fluctuations including anticipatory locomotor activity, anticipatory thirst and hunger, ovulation, osmoregulation, various gonadal functions, fever, and sickness behaviors (17–20).

While the route(s) traveled by diffusible signals from the SCN that support locomotor activity in animals bearing encapsulated SCN grafts remain(s) unknown, the newly discovered SCN-OVLTp stands as a potential candidate. We previously hypothesized that the flow of information is from SCN to OVLT (2). If so, then neurons of this small nucleus could secrete sufficient amounts of biologically important neuropeptides that travel to specialized nearby targets in the OVLT. The sensory neurons and fenestrated leaky blood vessels of this CVO could then relay humoral signals broadly via their neural and vascular outputs, thereby orchestrating circadian rhythms throughout the body.

While the foregoing hypotheses are plausible, at present, we do not know whether the SCN-OVLTp occurs in animals other than mouse and whether the direction of blood flow is from the SCN to the OVLT or vice versa. Here, we assessed the former question by studying the rat, and we next established the direction of blood flow

to assess the source and target within the SCN-OVLTp system. We then explored, in both sexes, day versus night regulation of blood flow in the portal vessels. Last, we asked whether AVP, a neuropeptide that has been identified as an output signal of the SCN, could enter portal vessels following systemic administration.

### **RESULTS**

### Anatomy of the rat SCN-OVLT portal pathway

To determine whether there exists a portal pathway between the SCN and OVLT in rat, we visualized the SCN and the vasculature of the ventral aspect of the brain using immunolabeling-enabled threedimensional imaging of solvent-cleared organs (iDISCO) cleared material, immunochemistry, and light sheet microscopy, as previously reported for the mouse (2) (see experimental pipeline in fig. S1). Figure 1 shows the major features of the volume between the two structures of interest. The scan in the left panel (Fig. 1A) provides a three-dimensional view of the location of the SCN and OVLT within the third ventricle. Next shown are the scans of three separate channels (Fig. 1B) identifying the SCN by its characteristic AVP neurons, the vasculature of the entire region labeled with collagen, and the arterial vasculature marked by smooth muscle actin (SMA) staining and a merged image of the three labels. The final panel shows the traced blood vessels that connect the SCN and OVLT. The results indicate that the major features of the rat portal pathway are similar to that of the mouse, with fine portal capillary vessels coursing along the floor of the third ventricle between the SCN and OVLT.

To demonstrate the precise course of the SCN-OVLTp vessels as they travel between the SCN and OVLT, we prepared serial horizontal optical scans through the dorso-ventral extent of the entire region (Fig. 1C). Triplets of images are shown from the ventral-most aspect of the SCN where portal vessels are found (Ci) through to the mid (Cii) and dorsal-most (Ciii) aspects of the SCN bearing these vessels. There are no portal vessels connecting to the SCN in the optical scan below and above these regions.

To guide the placement of the microscope for in vivo imaging, we performed precise measurements of the depth and extent of the SCN and OVLT above the optic chiasm, the distance between these structures, and the diameter of portal vessels (Fig. 2). Both nuclei of interest have complex shapes that change through their volumes in each axis. In the horizontal view, the portal vessels lie close to the midline of the brain (Fig. 2, A and B). In the sagittal view ( $z = 150 \, \mu m$ ), the distance between the SCN and OVLT is short, and both nuclei can be identified in the same light sheet microscope scan Fig. 2C, obviating the need to register the nuclei of interest against a template. The differing relative depth of the SCN and OVLT above the optic chiasm is shown in  $z = 2-\mu m$  views in Fig. 2 (D to G). Detailed measurements are provided in the legend of Fig. 2.

# In vivo two-photon imaging of the eGFP-AVP neurons in the SCN and the SON

We identified the SCN on the basis of the presence of dense endogenous enhaced green fluorescent protein (eGFP)–AVP–expressing neurons and fibers, using a modified version of our surgical approach to expose the ventral hypothalamus for in vivo imaging (21). As shown in Fig. 3 (A and B), the SCN lies medially to the SON and contains eGFP-AVP fluorescent neurons of much smaller size than those of the SON. In a few cases (n = 3), the SCNs and SONs were

exposed bilaterally (fig. S2A). On the basis of the anatomical characteristics of the portal system described above and on our knowledge of the SCN vasculature (22), we focused our in vivo imaging studies on the rostral aspect of the SCN.

### In vivo two-photon imaging of the SCN microvasculature

Vascular filling with Rhodamine 70-kDa dextran intravenously revealed a dense capillary network at this rostral region of the SCN, with only a few larger vessels noted (Fig. 3C). In agreement with the anatomical results, a distinct set of blood vessels coursed very close to the midline between the rostral aspect of the SCN and the caudal aspect of the OVLT (Fig. 3, D and E). A different example at lower magnification is shown in fig. S2B. The mean diameter of these portal vessels was  $11.4. \pm 0.6 \, \mu m$  ( $n = 30 \, vessels$ ).

In confirmation that these were portal venules and not arterioles, rats were first given an intravenous injection of the artery-specific dye Alexa Fluor 633 (23) to pre-label parenchymal arterioles (Fig. 4, A and D). Next, vascular filling was examined after intravenous administration of either Rhodamine 70-kDa (see examples shown in Fig. 4, B and C) or fluorescein isothiocyanate (FITC) 70-kDa dextrans (see examples shown in Fig. 4, D and E) to label all the microvasculature (see additional samples in fig. S2, C to F). Using this approach, we found only a few Alexa Fluor 633-labeled arterioles within the rostral SCN, and, in all cases (n=8), the rostrally running portal vessels were negative for Alexa Fluor 633. In summary, these properties of the in vivo-imaged material and their correspondence to the anatomical features and measurements shown in Figs. 1 and 2 confirm the identity of the SCN-OVLTp venules in vivo.

### Direction of blood flow is from SCN to OVLT

To determine the directionality of blood flow within the SCN-OVLTp, we performed fast sequential two-photon imaging of the acute loading phase of the portal vessels during intravenous infusion of Rhodamine 70-kDa dextran. This allows measurement of blood flow and directionality as the vessels are stained in real time with the intravascular dye. As shown in the two samples in Fig. 5, real-time measurement of intravascular loading of the SCN-OVLTp venules with the fluorescent dye showed that vessel staining started at caudal segments near the SCN and then rapidly moved rostrally toward the OVLT. A kymograph plot (Rhodamine 70-kDa dextran intensity as a function of time and distance along the portal vessels) confirmed the 12-bit of the portal vessels) confirmed the 12-bit of the portal vessels) confirmed the 12-bit of the portal vessels) confirmed the direction of dye movement from caudal (SCN) to rostral (OVLT) aspects. Similar results were observed in n = 6 independent experiments in separate rats. Thus, real-time measurement of the acute phase of fluorescent loading of the SCN-OVLTp vessels is evidence of flow from the SCN toward the OVLT.

In a second complementary approach, we measured blood flow direction and velocity by monitoring the movement of red blood cells (RBCs), as previously described (21). These appeared as moving dark spots in fluorescently labeled vessels in a segment of an imaged portal vessel. Representative images (Fig. 6, A to C) and a video (movie S1) compellingly show unidirectional movement of RBCs within the SCN-OVLTp system, running from a caudal to a rostral direction. This property was observed in every rat assessed (n = 10 females and n = 13 males). The mean basal blood flow velocity in the SCN-OVLTp was obtained from a subset of these rats (n = 16 vessels, 6 from females and 10 from males, n = 3 rats

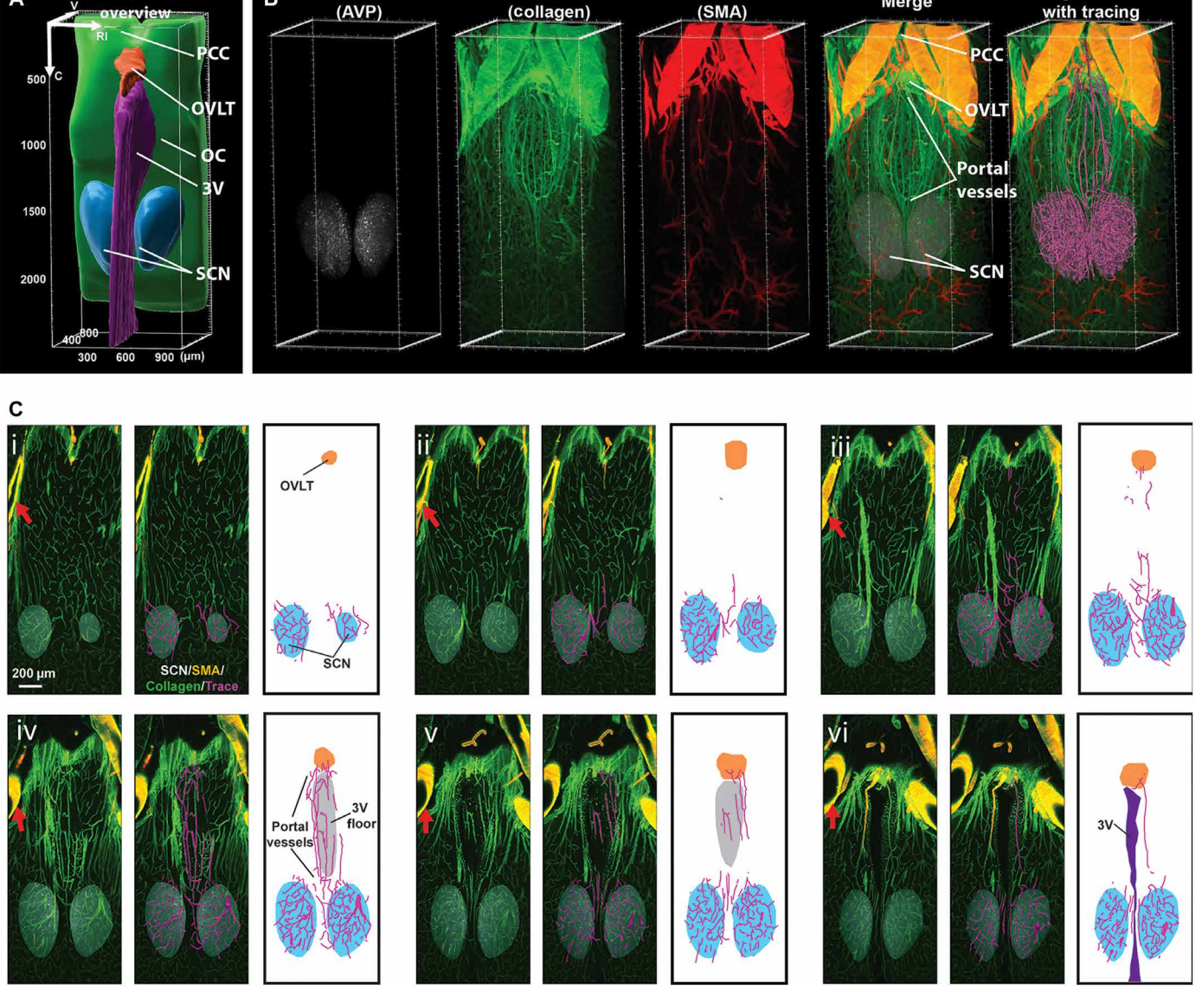
В

Horizontal

SCN

Merge overlaid

Merge



Vasculature

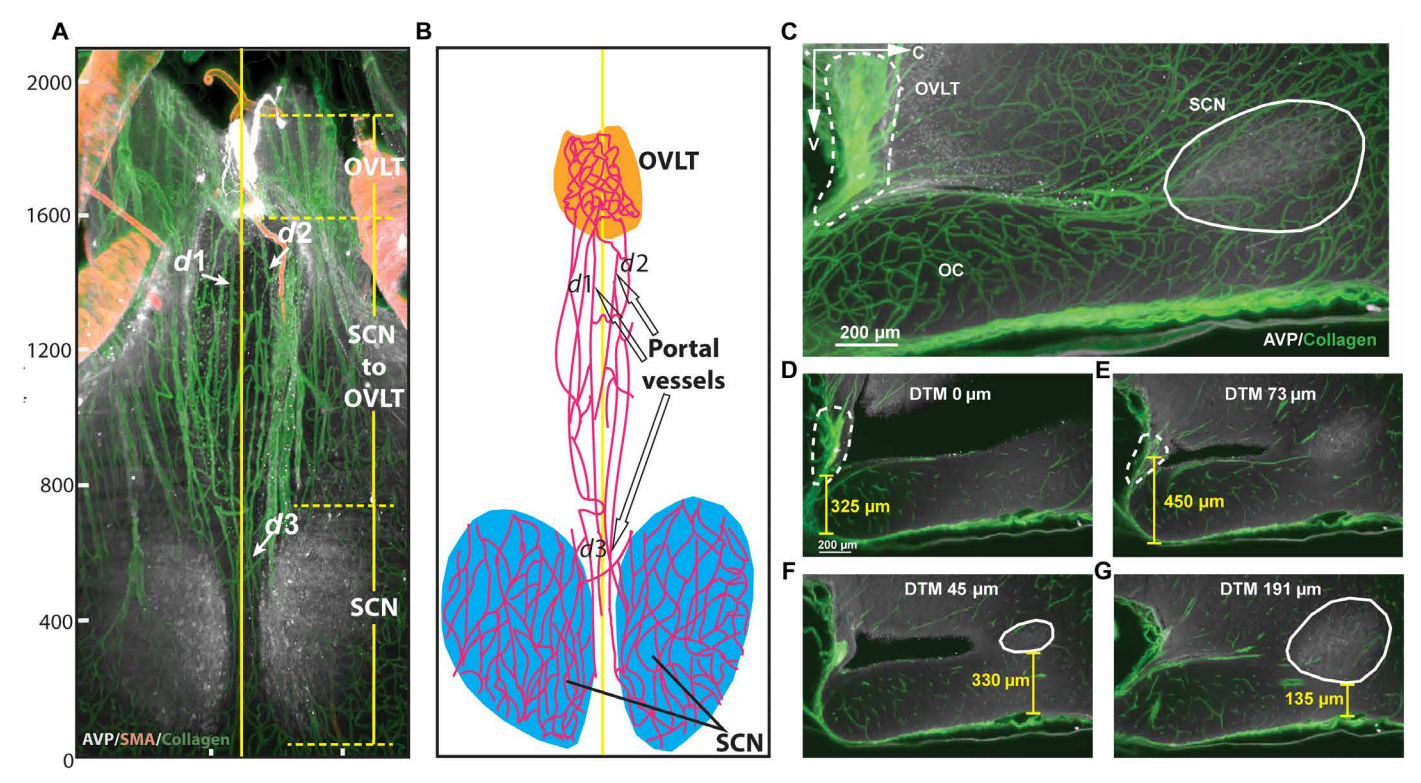
**Arteries** 

Fig. 1. Anatomy of the rat SCN-OVLT portal system. (A) Orientation of the horizontal scan of tissue shown in (B). In the rostro-caudal axis, the scanned volume extends from the prechiasmatic cistern (PCC) to the retrochiasmatic area (bregma, –0.84 to 1.72 mm) (38) including the full extent of the bilateral SCN. Reference axes denote the tissue orientation: C, caudal; V, ventral; RI, right. OVLT, orange; SCN, blue, 3V, magenta; OC, green. (B) Immunostaining and reconstruction of portal vessels connecting SCN and OVLT. The axis is for the same tissue depicted in (A). Panels (left to right) show the SCN identified by AVP staining, the vasculature labeled with collagen, arteries labeled with SMA, the merged image for the three markers, and the computer-assisted tracings of blood vessels of the merged image. (C) Portal capillaries from their most ventral to most dorsal aspect in serial 50-μm optical slices. The plates show image triplets as follows: left: merged AVP (white), collagen (green), and SMA (yellow); middle: blood vessel traces (magenta) superimposed on immunochemical results of the left panel; right: drawing identifying structures shown in the middle panel. Details of the serial plates are as follows: (i) initial appearance of the OVLT and portal blood vessels in the ventral SCN. (ii and iii) Portal vessels of the SCN extend rostrally from the SCN. (iv to vi) The rostrally running vessels of the SCN travel along the floor of the 3V and join the OVLT. For orientation in the serial sections, the red arrows (left of each triplet) point to a blood vessel that is seen in all photomicrographs demonstrating the continuity of the optical slices. 3V, purple; AVP, white; collagen, green; SMA, red; overlay of red/green, yellow; traces, magenta. OC, optic chiasm; OVLT, vascular organ of lamina terminalis; SMA, smooth muscle actin, 3V, third ventricle. See also fig. S1.

each sex) and was determined to be  $182.5 \pm 19.9 \,\mu\text{m/ms}$ . There were no significant differences between the sexes in either velocity or diameter [ $P > 0.54 \, (t = 0.62)$  and  $P > 0.35 \, (t = 0.97)$ , respectively, unpaired t test]. An opposite direction of blood flow, from rostral to caudal, was observed in neighboring lateral lying vessels (movie S2).

# Time of day affects blood flow in the SCN-OVLT portal system

To determine whether the rate of blood flow within the SCN-OVLT portal system varies according to the time of day, we compared blood flow at ~midday [zeitgeber time (ZT) 5 to 7] and ~midnight (ZT 17 to 19). As controls, and to determine whether day-night differences



**Fig. 2. Size and locations of the SCN, OVLT, and portal vessels. (A)** Vasculature of the SCN and OVLT region in a 100-μm optical horizontal slice. The rostro-caudal (R-C) extent of the OVLT is 270 μm; the distance between caudal OVLT and rostral SCN is 730 μm; the R-C extent of SCN is 640 μm. The vertical solid yellow line at 490 μm on the left-right axis indicates the midline of the brain. Portal vessels lie within 100 μm of the midline. The diameter (d) of portal vessels at d1, d2, and d3 are as follows: d1 = 11 μm, d2 = 13 μm, and d3 = 8 μm. (**B**) The drawing identifies structures shown in (A) and highlights the traced portal vessels. The designations d1, d2, and d3 refer to the portal vessels shown in (A). (**C**) Sagittal optical slice (z = 150 μm) of the SCN-OVLT region. (**D**) The shortest distance from OVLT to the ventral OC is 325 μm and occurs at the midline. (**E**) The greatest distance from ventral OVLT to ventral OC is 450 μm, and, at this point, the distance to midline (DTM) is 73 μm. (**F**) The greatest distance between ventral SCN and ventral OC is 330 μm, and, here, the DTM is 191 μm. For (D) to (G), z = 2 μm. The other abbreviations are as in Fig. 1.

in blood flow were specific to the portal vessels, we also obtained measurements from nearby vessels that, based on their anatomical location and orientation, were not part of the portal system. Data were analyzed using two-way analysis of variance (ANO-VA; factors: time of day  $\times$  portal versus nearby vessel type). We found that RBC velocity in portal vessels, but not in nearby nonportal vessels, was significantly faster at night than in the day (time of day:  $F_{DF} = 9.5$ , P = 0.004; vessel type:  $F_{DF} = 1.0$ , P = 0.32; interactions:  $F_{DF} = 15.6$ , P = 0.001; portal vessels: ZT 17 to 19 versus ZT 5 to 7; P < 0.0001, Tukey post hoc test; Fig. 6D]. Conversely, no time differences in blood flow were observed in nonportal vessels (ZT 17 to 19 versus ZT 5 to 7; P = 0.99, Tukey post hoc test). In addition, there were no time-of-day differences in portal vessel diameter between these time points neither in portal vessels (P = 0.74, Tukey post hoc test) nor in non-portal vessels (P = 0.74, Tukey post hoc test; Fig. 6D). Moreover, we found no significant correlation between portal vessel blood flow velocity and diameter for either vessel type (portal vessels:  $r^2 = 0.002$ , P = 0.79; non-portal vessels:  $r^2 = 0.17$ , P = 0.17; Fig. 6E). Last, systemic mean arterial pressure (MAP) did not differ between day and night periods [P = 0.95 (t = 0.06), unpaired *t* test; Fig. 6F].

# Intravenously infused AVP travels within the SCN-OVLT portal system

To determine whether a functionally relevant neuropeptide can penetrate and circulate within the SCN-OVLTp system, we systemically infused a fluorescently tagged AVP (AVP<sub>FL</sub>). An intravenous infusion of AVP<sub>FL</sub> resulted in a rapid increase in fluorescent signal within the SCN-OVLTp vessels (Fig. 7A). Neither vessel diameter nor velocity was significantly changed by the infusion of AVP<sub>FL</sub> [P > 0.78 (t = 0.29) and P > 0.20 (t = 1.88), respectively, paired t test; Fig. 7D), although a trend to an increase in velocity was noted. In a separate set of experiments, we tested whether the infusion of AVP<sub>FL</sub> could affect systemic blood pressure. As summarized in Fig. 7 (E and F), AVP<sub>FL</sub> failed to affect MAP [P = 0.62 (t = 0.51), paired t test]. As a positive control, we tested in a subset of cases the effects of phenylephrine (Phe) and show, as expected, that Phe significantly increased MAP [P < 0.01 (t = 11.02), paired t test].

### **DISCUSSION**

The present study demonstrates unequivocally that, in portal vessels, blood flows from the SCN to the OVLT via a vascular portal pathway. Blood flow in the SCN-OVLTp displays daily oscillations.

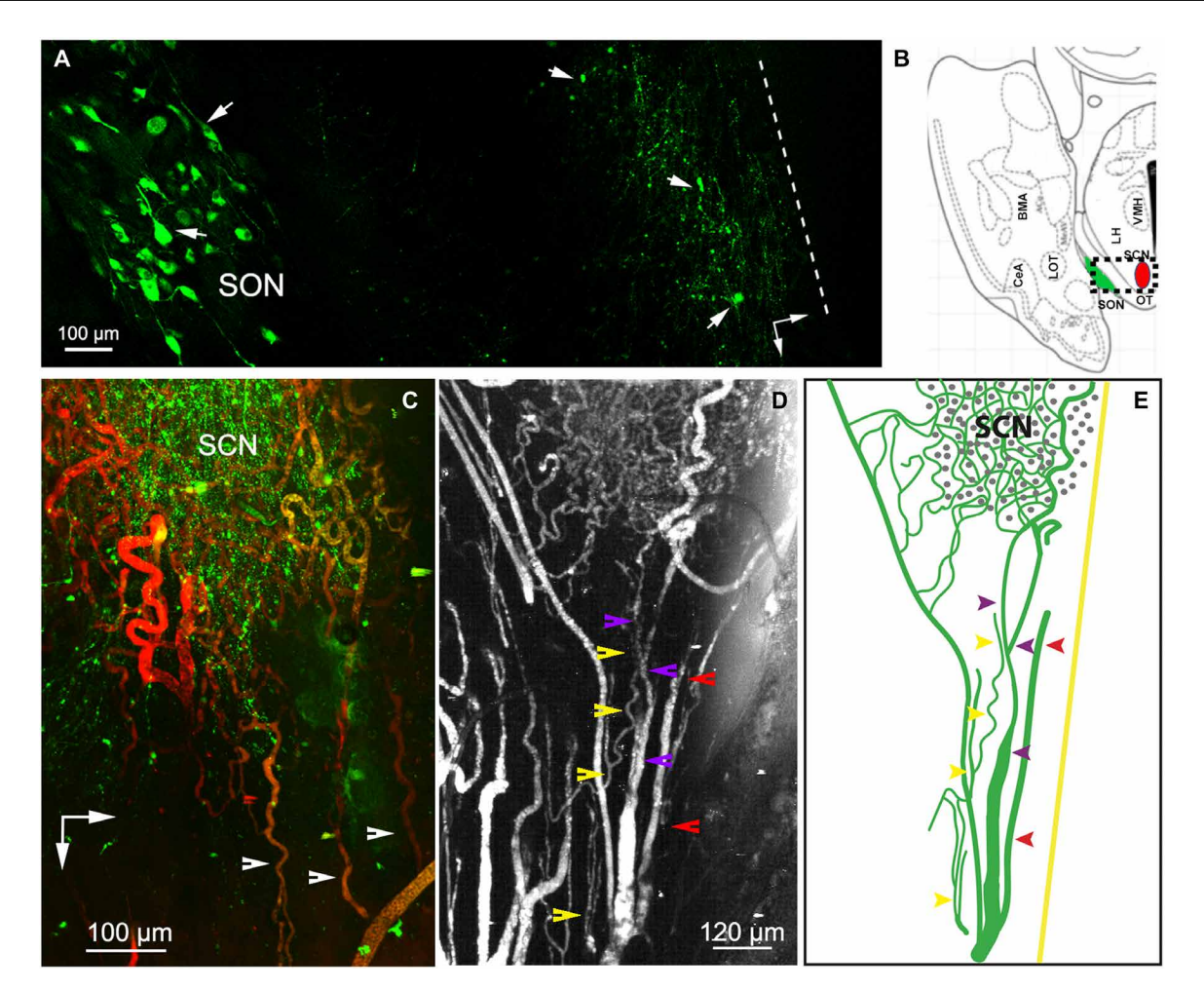


Fig. 3. In vivo two-photon imaging of the SCN microvasculature. (A) Composite of sequential mediolateral images (16× objective) showing eGFP-AVP neurons and fibers in the right SON and SCN of an eGFP-AVP rat (arrows). Note the large magnocellular neurons in the SON. Dashed line represents the apparent midline. Vertical and horizontal arrows point rostrally and medially, respectively. (B) Cartoon of the brain atlas (38) showing a horizontal section of the brain and the area imaged (square). The SON and SCN are highlighted in green and red, respectively. (C) In vivo two-photon imaging of the rostral aspect of the SCN following Rhodamine 70-kDa dextran infusion (intravenous). Note the dense capillary network within the SCN (containing dense endogenous eGFP-AVP fluorescence) and the horizontal, rostro-caudally running vessels (arrowheads). Vertical and horizontal arrows point rostrally and medially, respectively. (D) Representative FITC 70-kDa dextran–labeled capillary vessels of the SCN and the rostro-caudally running portal vessels lying close to the midline (arrowheads; each color indicates a separate vessel). The image is shown in black and white to enhance visualization. (E) Drawing identifying the key structures shown in the middle panel (D). The yellow straight line represents the location of the brain midline. See also fig. S2. CeA, central nucleus of amygdala; OT, optic track; LOT, lateral olfactory tract; LH, lateral hypothalamic area; BMA, basomedial amygdaloid nucleus-anterior part; VMH, ventromedial hypothalamic nucleus.

In addition, our studies show that AVP, once entering the SCN microcirculation, can access and flow within the SCN-OVLTp. Whether AVP of SCN origin flows within the portal system remains to be determined.

As noted in Introduction, transplants of the copolymerencapsulated SCN that permit diffusion of neurosecretions but prevent establishment of neural connections confirm that the SCN produces sufficient diffusible neurosecretions to sustain circadian locomotor rhythms (11). The conclusion is supported by in vitro coculture studies indicating that AVP, VIP, and GRP from a wildtype SCN can drive rhythms in a target tissue of an SCN-deficient mutant animal (15). Together, this small nucleus, composed of ~20,000 small neurons, generates chemical secretions of sufficient concentration to support circadian rhythms in nearby targets. Most importantly, the present work points to the SCN-OVLTp as a route whereby such signals can travel.

Our findings are also consistent with prior work on the possible target site of a diffusible signal. The weight of evidence indicates that the target of diffusible SCN secretion lies nearby this nucleus. Thus, SCN transplants are successful in restoring rhythms when placed anywhere within the third ventricle (24) but not in remote sites. Calculations on the distance that diffusible SCN neurosecretions could travel suggest that the humoral signals have to act on a nearby target (25). The OVLT, lying at a distance of 385  $\mu m$  from the SCN in mouse (2) and 730  $\mu m$  in the rat, meets the criterion.

We found that the rate of blood flow in this portal system is higher during nighttime compared to daytime, supporting the notion that this phenomenon is amenable to modulation by rhythmic circadian

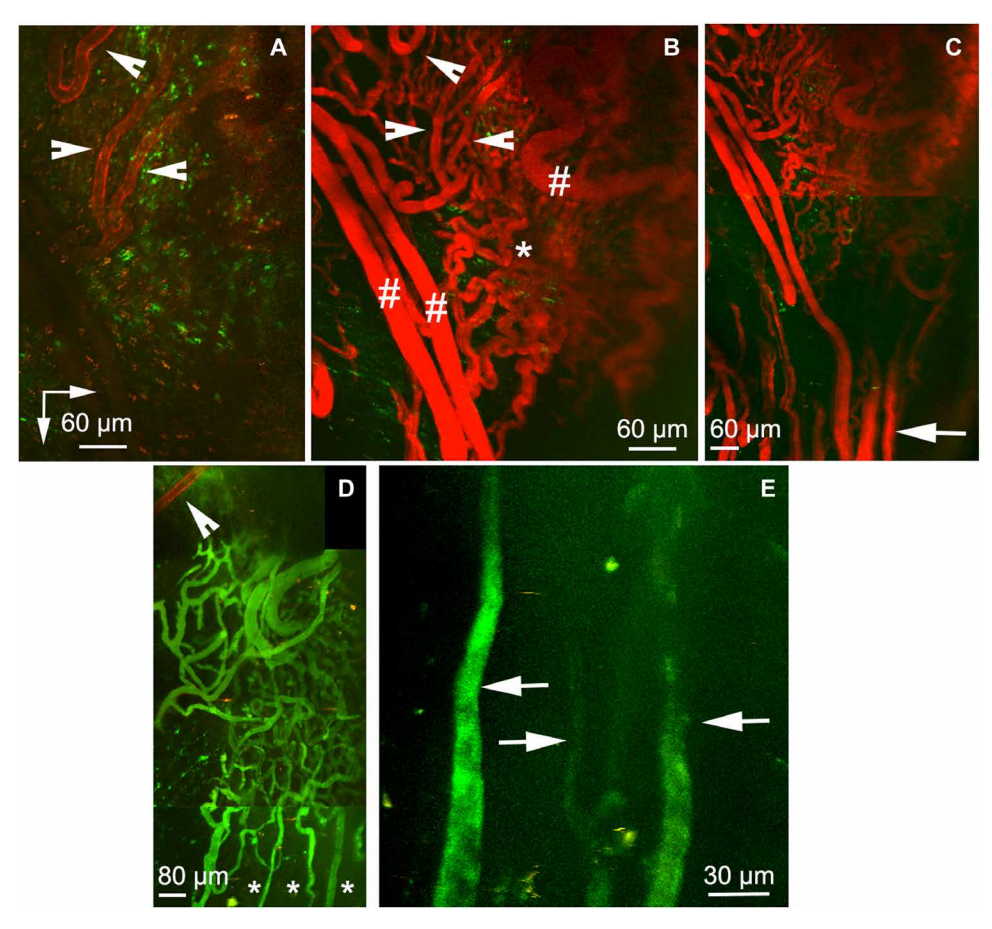


Fig. 4. The SCN-OVLT portal vessels are venules and not arterioles. (A) Two-photon image of the rostral aspect of the SCN after an intravenous injection of Alexa Fluor 633. Few arterioles show positive staining (red, arrowheads). (B) Same region shown in (A), shown at a lower magnification following labeling of the entire microcirculation with Rhodamine 70-kDa dextran infusion (intravenous). Arrowheads point to the arterioles shown in (A). The asterisk and hashtags indicate capillaries and venules, respectively, within the SCN. (C) Composite of images at lower magnification (4x objective) of the same region shown in (A) and (B) to show the bundle of portal vessels labeled with Rhodamine 70-kDa dextran (arrow). Note the absence of Alexa Fluor 633 staining in the SCN capillary network or any other vessels running rostrally from the SCN. (D) Two-photon image composite of the rostral SCN showing an Alexa Fluor 633-stained vessel (arrowhead) and vessels subsequently stained with fluorescein isothiocyanate (FITC) 70-kDa dextran (intravenous). Note the scarce Alexa Fluor 633 staining at this SCN level (arrowhead) and that the rest of the stained vasculature shows only FITC 70-kDa dextran staining. Asterisks indicate initial segment of a few portal vessels. (E) Image taken more rostrally than (D) and shown at higher magnification to better show the portal vessels stained with FITC 70-kDa dextran but lacking Alexa Fluor 633 staining (arrows). Vertical and horizontal arrows in a point rostrally and medially, respectively. See also fig. S2.

signals. Our results showed that changes in blood flow occurred in the absence of changes in portal vessel diameter. Given that these are non-resistive vessels, these data suggest that mechanisms other than changes in the portal vessel diameter themselves contribute to blood flow regulation in this system. These could include circadian variations in the release and actions of vasoactive substances within the SCN (e.g., AVP, VIP, and GRP) (2) that could result in circadian pressure differential between the capillary beds in SCN and OVLT, thus leading to changes in blood flow in the portal system. Alternatively, circadian variations in systemic blood pressure could contribute to day-night differences in portal blood flow. However, our data showing similar MAP values at the day versus nighttime points argue against the latter. Last, daily variations in venous drainage at the level of the OVLT could also contribute to concomitant changes in portal blood flow rates. We can only speculate on the functional significance of changes in rate of blood flow. Possibly, day-night differences in blood flow result in concomitant fluctuations in the signals

transported to the neurons and leaky blood vessels of the OVLT and thence to its extensive distal targets (17). In addition, given that the capillaries contribute substantially to hemodynamic resistance (26), another possibility is that the relative capillary resistance between OVLT and SCN changes between day and night thereby driving daily variation.

Of immediate interest is the possible signal carried by the portal vasculature, a question that is not addressed in the present study, as many neurosecretions may course within the portal pathway. We do show, however, that systemically infused fluorescently tagged AVP travels within the portal vessels. We focused on AVP for several reasons. First, the OVLT has receptors for AVP (27). Furthermore, AVP is produced within the SCN with a daily rhythm, is a well-established SCN output signal [reviewed in (12, 27)], and can act in a diffusible manner (11–15, 24, 28). Rhythms in CSF AVP are lost in the absence of rhythms of a molecular clock controlling AVP in the SCN (29, 30). Last, AVP plays an important role as an

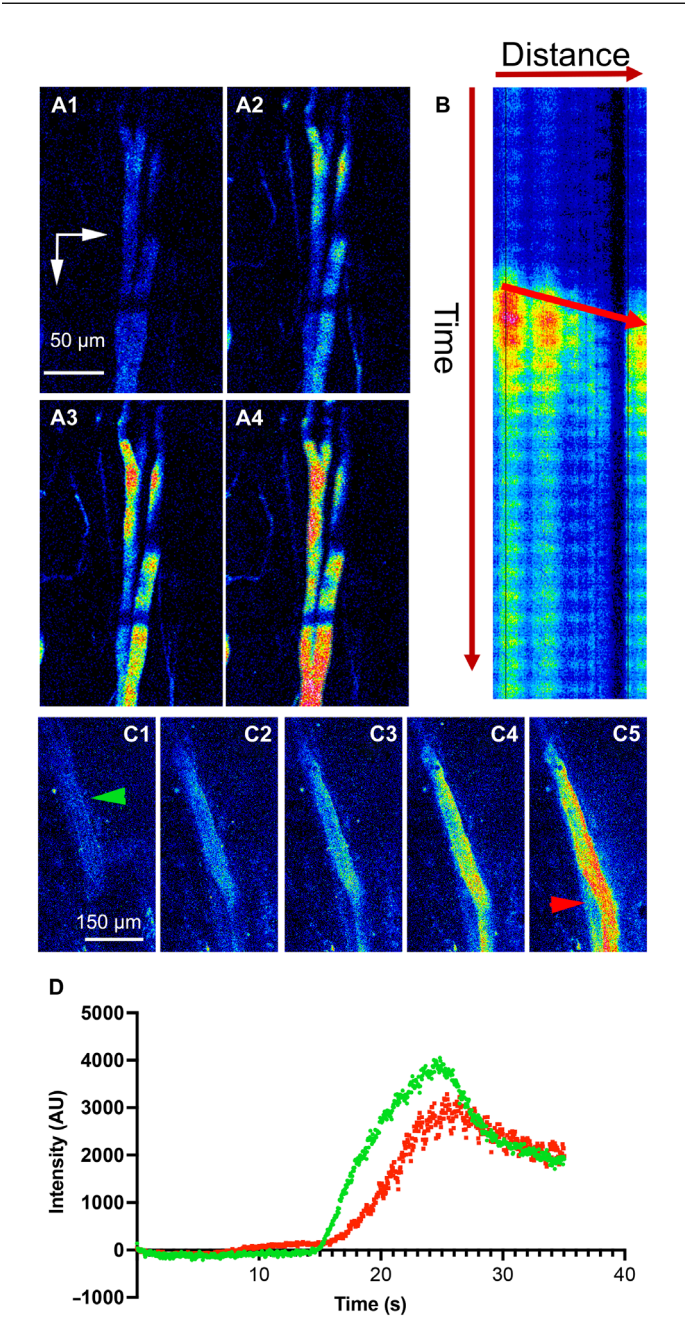


Fig. 5. Acute loading of the SCN-OVLT portal system supports blood flowing from SCN toward the OVLT. (A) Sequential time-series two-photon imaging (A1 to A4) of the acute loading phase of the portal vessels during Rhodamine 70-kDa dextran intravenous infusion (pseudo-color). Note that loading starts at caudal segments and then moves rostrally. (B) Kymograph plot of Rhodamine 70-kDa dextran intensity as a function of time (vertical arrow) and distance (horizontal arrow, from caudal to rostral) along the portal vessels. The arrow within the graph indicates direction of movement over time, indicating a flow from the SCN (caudal) to the OVLT (rostral) direction. (C) Sequential time-series two-photon imaging of a different portal vessel during the acute loading phase (Rhodamine 70-kDa dextran intravenous infusion). Green and red arrowheads indicate segments where plots in (D) were generated. (D) Plot of portal vessel fluorescence intensity over time taken at a caudal (green) and rostral (red) segments from the vessel shown in (C). Note the delayed increased fluorescence in the rostral segment, supporting blood flow in a caudal-to-rostral direction, from the SCN toward the OVLT. Vertical and horizontal arrows in (A1) point rostrally and medially, respectively. AU, arbitrary units.

intercellular communication signal (31, 32) and is essential for SCN network synchrony and rhythmicity (9). While our results convincingly show that systemic AVP can access the SCN-OVLTp circulation, we acknowledge that this does not provide direct evidence that locally released AVP within the SCN would also access this portal system.

Gizowski et al. (33) showed that optogenetic stimulation of SCN-AVP axon terminals within the OVLT excited OVLT neurons in an AVP-dependent manner, supporting a functional neuronal AVP pathway from the SCN to the OVLT. Together with the present study, these results support the presence of two AVP-mediated communication channels between the SCN and the OVLT (a neuronal and humoral) acting at very different spatio-temporal scales (fast and spatially precise versus slow and spatially diffuse, respectively). Whether these two channels mediate different AVP functions within the SCN will need to be determined in future studies. Alternatively, it is important to consider that AVP reaching the OVLT via the portal system could also access the ventricular system, thereby signaling distant targets beyond the OVLT proper.

In summary, using a combination of anatomical and in vivo imaging techniques, we show that the SCN-OVLTp is a functional portal system that is present in both sexes and potentially carries circadian information from the SCN toward the OVLT. The SCN-OVLTp is a previously unknown notable route and target for diffusible output signals from the brain clock in the SCN. The major anatomical features of the SCN-OVLTp pathway of the rat resemble that of previously described in the mouse (2) and suggest that this pathway, like the pituitary portal system, is a common feature in the mammalian brain.

### **MATERIALS AND METHODS**

### **Animals**

Male and female heterozygous transgenic eGFP-AVP Wistar rats (34) (250 to 490 g, 8 to 16 weeks old) were used (n = 12 females and n = 16 males for in vivo studies; n = 2 females and n = 2 males for iDISCO anatomical studies). For in vivo measurements of systemic blood pressure, Wistar rats (300 to 320 g, 9 to 10 weeks old, n = 8 males) were used. Rats were housed (two per cage) under constant temperature (22°  $\pm$  2°C) and humidity (55  $\pm$  5%) on a 12-hour light cycle [lights on, 08:00 to 20:00 (ZT 0 to 12)]. In a subset of studies, rats (n = 4) were put on a reversed light cycle (lights on: 20:00 to 08:00). For anatomical studies, brains were shipped to Columbia University. All performed experiments were approved by the Georgia State University and Auburn University Institutional Animal Care and Use Committees (IACUC) and carried out in agreement with the IACUC guidelines. At all times, animals had ad libitum access to food and water, and all efforts were made to minimize suffering and the numbers of animals used for the study.

# iDISCO clearing, light sheet microscopy, image processing, and vascular tracing

The iDISCO protocol used in this study is modified from (35). The tissue was labeled with anti-AVP antibody to delineate the SCN, anti-SMA for arteries, and anti-type IV collagen for all blood vessels. Light sheet microscopic images were acquired with a LaVision Ultramicroscope II. Blood vessel tracing was done in Imaris and

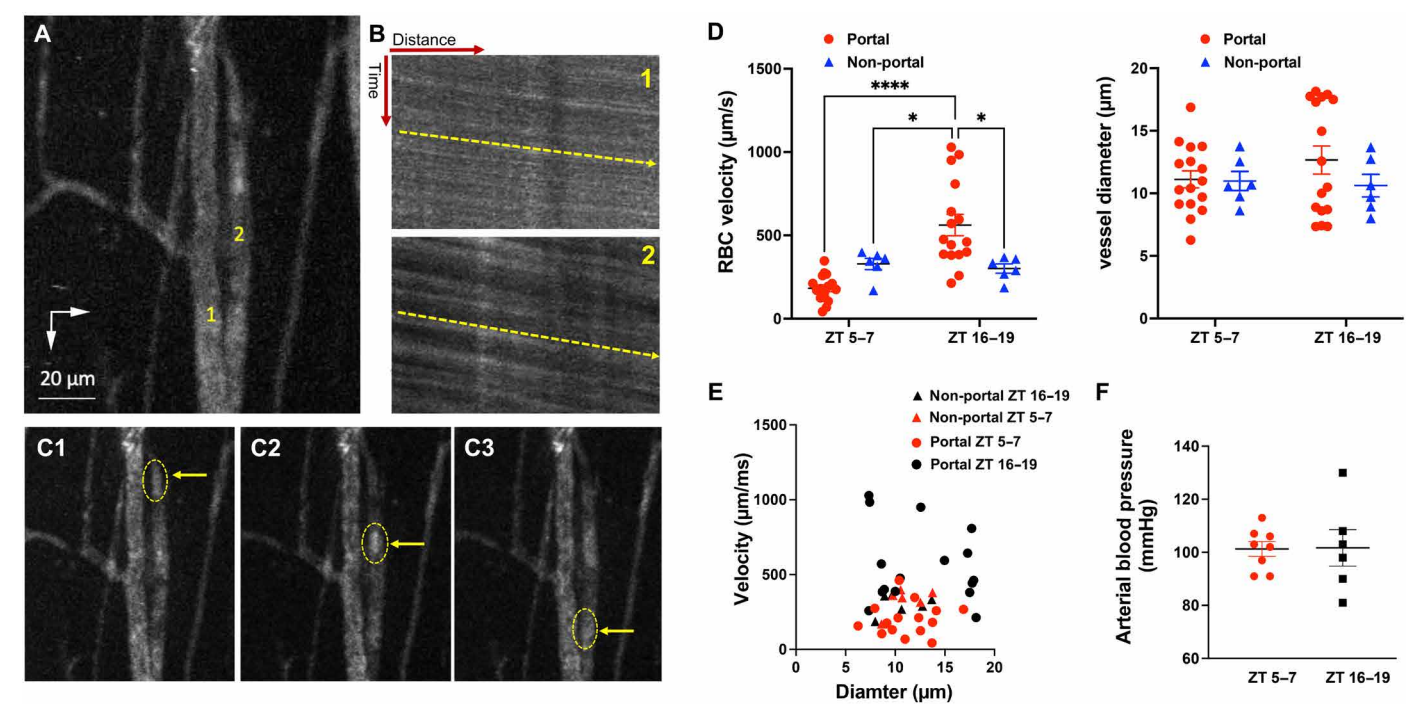


Fig. 6. Measurements of RBC movement within the SCN-OVLT portal system support blood flowing from SCN toward the OVLT and increase blood flow during the night phase. (A) Two-photon imaging of a pair of SCN-OVLT portal vessels (1 and 2) used to measure red blood cell (RBC) movement. (B) Kymograph plots of Rhodamine 70-kDa intensity as a function of time (vertical) and distance (horizontal, caudal to rostral) along the portal vessels 1 and 2 from (A). Note the streak slopes (yellow arrows) showing movement from caudal to rostral over time. (C) Sequential time-series two-photon imaging (C1 to C3) of the portal vessels shown in (A), showing a group of RBCs (oval, yellow arrow) moving progressively in a caudal-to-rostral direction. (D) Summary of RBC velocities (left) and vessel diameters in SCN-OVLT portal vessels (red circles) during the day (ZT 5 to 7, n = 16 vessels from six rats) and night (ZT 17 to 19, red, n = 16 vessels from five rats) as well as data from non-portal vessels (blue triangles) during the same day/night time points (n = 6 vessels from six rats (one vessel per rat) at each time point. (E) Plots of RBC velocities as a function of vessel diameter at day and night phases, for portal (circles) and non-portal (triangles) vessels showing a lack of significant correlation in both cases ( $r^2 = 0.002$ , P = 0.79; and  $r^2 = 0.17$ , P = 0.17, respectively, chi-square tests). (F) No significant differences in baseline MAP were observed between day (ZT 5 to 7, n = 8 rats) and night (ZT 17 to 19, n = 6 rats) phases. Vertical and horizontal arrows in (A1) point rostrally and medially, respectively. \*P < 0.05 and \*\*\*\*P < 0.0001 (Tukey post hoc test). Error bars represent ±SEM.

Vessulucida360. The SCN-specific labeling by AVP allows identification of the SCN without registration.

### In vivo two-photon imaging of the SCN

A modified version of the transpharyngeal surgical approach to expose the ventral surface of the brain was used (36) in conjunction with in vivo two-photon imaging as previously described (21). The exposed SCN (identified by the presence of eGFP-AVP neurons) was imaged under a two-photon microscope excited with a Ti:Sapphire tuned at 860 nm and scanned with resonant galvanometers through a 16× (numerical aperture of 0.8) water immersion objective or a 4× (numerical aperture of 0.13) objective. Galvanometric scanning and resonant scanning (for imaging vessel dye loading and for RBC velocity) were controlled by PrairieView.

# In vivo imaging of the arterial and venous filling phases of the SCN vasculature

The artery-specific dye Alexa Fluor 633 (23) [1 to 2 mg/kg injected intravenously (iv), femoral vein] 1.5 hours before two-photon imaging recordings was used to label and differentiate SCN arterioles from venules. Time-lapse imaging was performed using the resonant scanning mode at 30-Hz frame rate,  $512 \times 512$  pixels during the intravenous administration of Rhodamine or FITC 70-kDa

dextrans (20 mg/ml, 200 nl per rat). Where noted, a fluorescently labeled form of AVP (FAM-AVP, AnaSpec) was infused in a similar way to the dextrans.

# In vivo quantification of blood flow rate and direction in the SCN-OVLT portal system

The SCN-OVLTp was identified as vessels originating from a dense SCN capillary network that run rostrally close to the midline toward the OVLT and that were Rhodamine/FITC 70-kDa dextran–positive and Alexa Fluor 633 (an artery/arteriole specific dye)–negative. Blood velocity was calculated by monitoring the movement of RBCs, which appeared as moving dark spots in fluorescently labeled vessels). Highspeed (500 to 1000 Hz, 5 to 10 s) resonant scanning images were obtained from a small region of interest (on average  $150 \times 25$  pixels) drawn across the width of the vessel of interest. Velocity kymographs were constructed in ImageJ and used to determine directionality.

### Measurements of systemic blood pressure

Animals were anesthetized with urethane (1.4 g/kg body weight, intraperitoneally). The depth of anesthesia was verified by the lack of response to tail and toe pinches, and one-third of the original dose was administered as needed. Blood pressure was acquired through an intra-arterial catheter in anesthetized animals. Briefly, the

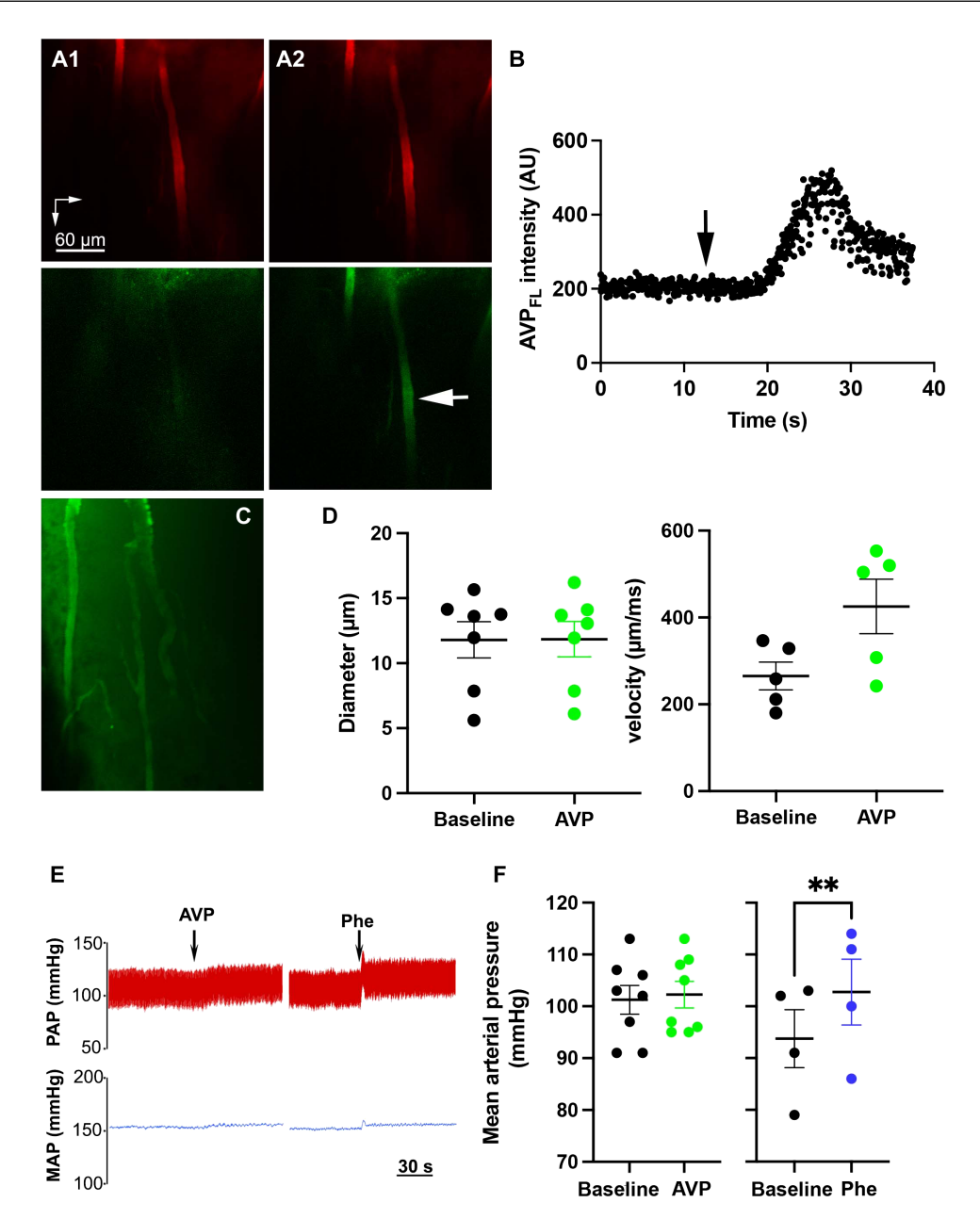


Fig. 7. A fluorescent form of AVP (AVP<sub>FL</sub>) infused into the circulation can enter and travel within the SCN-OVLT portal system. (A) Two-photon images of SCN-OVLT portal vessels preloaded with Rhodamine 70-kDa dextran intravenous infusion (red, top panels) before (A1) and after (A2) systemic infusion of AVP<sub>FL</sub> (green, bottom panels). Arrow points to the segment of the portal vessels used for measurements shown in (B). (B) Plot of AVP<sub>FL</sub> intensity over time following its intravenous infusion (arrow). (C) Two-photon image of SCN-OVLT portal vessels in another rat showing the presence of AVP<sub>FL</sub> inside the vessels. (D) Summary plots showing SCN-OVLT portal vessel diameter (left, n = 7 vessels from seven rats) and blood flow velocity [right, n = 5 vessels from five rats (in two rats, blood flow velocity could not be measured reliably)] at baseline and following the AVP<sub>FL</sub> infusion. (E) Representative traces displaying pulsatile arterial pressure (PAP) and MAP in an anesthetized rat. The traces depict the effects of an intravenous bolus injection of AVP<sub>FL</sub> (20  $\mu$ M) and phenylephrine (Phe; 1  $\mu$ g/ $\mu$ I) on PAP and MAP before and after drug administration, as indicated by the arrows. (F) Summary data showing MAP levels before and after the injection of AVP<sub>FL</sub> (left, n = 8 rats) and Phe (right, n = 4 rats). Note the absence of changes in MAP in response to AVP<sub>FL</sub> intravenous injections. Conversely, a significant increase in MAP was observed in the same rats in response to Phe. \*\*P < 0.01, paired t test. Vertical and horizontal arrows in (A1) point rostrally and medially, respectively. Error bars represent  $\pm$ SEM.

femoral artery and vein were isolated from the connective tissue, and a heparin-filled catheter was inserted in each for arterial blood pressure recordings and intravenous administration of drugs, respectively. The arterial catheter was connected to a pressure transducer (model SP 844, Memscap AS, Norway) coupled to an amplifier

for data acquisition (Bridge Amp/PowerLab 4/35, ADInstruments, Australia). After 20 min of baseline recording, vasopressin-fluor (20  $\mu$ M, 0.5 ml, in bolus iv) and Phe (1  $\mu$ g/1  $\mu$ l, 0.5 ml, in bolus iv) were administered to observe any changes in blood pressure. A minimum interval of 10 min was established to ensure cardiac

parameters returned to baseline levels before the next administration (two injections were performed in each animal). Basal blood pressure in urethane-anesthetized rats was also acquired during the dark phase using the described procedure.

### Statistical analysis

Statistical analyses were performed using Prism 8 (GraphPad, CA, USA). Quantitative data were expressed as the means  $\pm$  SEM. No statistical methods were used to predetermine sample sizes, but sample sizes in the current study were similar to our previous reports (21, 37). Data were analyzed by two-way ANOVA followed by Tukey post hoc tests. When appropriate, as indicated in the text, paired or unpaired t test (two-sided in all cases) was used. Chisquare tests were used to establish significant correlations. Data distribution was assumed to be normal, although this was not formally tested. Values were considered significantly different at P < 0.05. Statistical details of experiments can be found in the figure legends.

### **Supplementary Materials**

This PDF file includes:

Figs. S1 and S2 Legends for movies S1 and S2

Other Supplementary Material for this manuscript includes the following: Movies S1 and S2

### **REFERENCES AND NOTES**

- G. T. Popa, U. Fielding, Hypophysio-portal vessels and their colloid accompaniment. J. Anat. 67, 227–232.221 (1933).
- Y. Yao, A. B. Taub, J. LeSauter, R. Silver, Identification of the suprachiasmatic nucleus venous portal system in the mammalian brain. *Nat. Commun.* 12, 5643 (2021).
- G. W. Harris, Pituitary-hypothalamic mechanisms. AMA Arch. Neurol. Psychiatry 73, 124–126 (1955).
- E. E. Abrahamson, R. Y. Moore, Lesions of suprachiasmatic nucleus efferents selectively affect rest-activity rhythm. Mol. Cell. Endocrinol. 252, 46–56 (2006).
- L. J. Kriegsfeld, R. K. Leak, C. B. Yackulic, J. LeSauter, R. Silver, Organization of suprachiasmatic nucleus projections in Syrian hamsters (*Mesocricetus auratus*): An anterograde and retrograde analysis. *J. Comp. Neurol.* 468, 361–379 (2004).
- L. P. Morin, N. Goodless-Sanchez, L. Smale, R. Y. Moore, Projections of the suprachiasmatic nuclei, subparaventricular zone and retrochiasmatic area in the golden hamster. *Neuroscience* 61, 391–410 (1994).
- M. Prager-Khoutorsky, C. W. Bourque, Anatomical organization of the rat organum vasculosum laminae terminalis. *Am. J. Physiol. Regul. Integr. Comp. Physiol.* 309, R324–R337 (2015).
- H. J. Romijn, A. A. Sluiter, C. W. Pool, J. Wortel, R. M. Buijs, Evidence from confocal fluorescence microscopy for a dense, reciprocal innervation between AVP-, somatostatin-, VIP/PHI-, GRP-, and VIP/PHI/GRP-immunoreactive neurons in the rat suprachiasmatic nucleus. Eur. J. Neurosci. 9, 2613–2623 (1997).
- Y. Shan, J. H. Abel, Y. Li, M. Izumo, K. H. Cox, B. Jeong, S. H. Yoo, D. P. Olson, F. J. Doyle III, J. S. Takahashi, Dual-color single-cell imaging of the suprachiasmatic nucleus reveals a circadian role in network synchrony. *Neuron* 108, 164–179.e7 (2020).
- S. Varadarajan, M. Tajiri, R. Jain, R. Holt, Q. Ahmed, J. LeSauter, R. Silver, Connectome of the suprachiasmatic nucleus: New evidence of the core-shell relationship. eNeuro 5, 0205–0218 (2018).
- R. Silver, J. LeSauter, P. A. Tresco, M. N. Lehman, A diffusible coupling signal from the transplanted suprachiasmatic nucleus controlling circadian locomotor rhythms. *Nature* 382, 810–813 (1996).
- R. M. Buijs, G. Hurtado-Alvarado, E. Soto-Tinoco, Vasopressin: An output signal from the suprachiasmatic nucleus to prepare physiology and behaviour for the resting phase. J. Neuroendocrinol. 33, e12998 (2021).
- 13. J. LeSauter, R. Silver, Output signals of the SCN. *Chronobiol. Int.* **15**, 535–550 (1998).
- J. D. Li, W. P. Hu, Q. Y. Zhou, The circadian output signals from the suprachiasmatic nuclei. *Prog. Brain Res.* 199, 119–127 (2012).

- E. S. Maywood, J. E. Chesham, J. A. O'Brien, M. H. Hastings, A diversity of paracrine signals sustains molecular circadian cycling in suprachiasmatic nucleus circuits. *Proc. Natl. Acad.* Sci. U.S.A. 108, 14306–14311 (2011).
- M. J. McKinley, I. J. Clarke, B. J. Oldfield, "Circumventricular organs" in The Human Nervous System (Academic Press, ed. 2, 2004), pp. 562–591.
- M. J. McKinley, D. A. Denton, P. J. Ryan, S. T. Yao, A. Stefanidis, B. J. Oldfield, From sensory circumventricular organs to cerebral cortex: Neural pathways controlling thirst and hunger. J. Neuroendocrinol. 31, e12689 (2019).
- C. Gizowski, C. W. Bourque, Sodium regulates clock time and output via an excitatory GABAergic pathway. Nature 583, 421–424 (2020).
- B. Coiffard, A. B. Diallo, S. Mezouar, M. Leone, J. L. Mege, A tangled threesome: Circadian rhythm, body temperature variations, and the immune system. *Biology* 10, (2021).
- J. W. Everett, C. H. Sawyer, A neural timing factor in the mechanism by which
  progesterone advances ovulation in the cyclic rat. *Endocrinology* 45, 581–595 (1949).
- R. K. Roy, F. Althammer, A. J. Seymour, W. Du, V. C. Biancardi, J. P. Hamm, J. A. Filosa, C. H. Brown, J. E. Stern, Inverse neurovascular coupling contributes to positive feedback excitation of vasopressin neurons during a systemic homeostatic challenge. *Cell Rep.* 37, 109925 (2021).
- Y. Yao, I. K. Green, A. B. Taub, R. Tazebay, J. LeSauter, R. Silver, Vasculature of the suprachiasmatic nucleus: Pathways for diffusible output signals. *J. Biol. Rhythms* 38, 571–585 (2023).
- Z. Shen, Z. Lu, P. Y. Chhatbar, P. O'Herron, P. Kara, An artery-specific fluorescent dye for studying neurovascular coupling. *Nat. Methods* 9, 273–276 (2012).
- J. LeSauter, P. Romero, M. Cascio, R. Silver, Attachment site of grafted SCN influences precision of restored circadian rhythm. J. Biol. Rhythms 12, 327–338 (1997).
- U. Schibler, J. Ripperger, S. A. Brown, Peripheral circadian oscillators in mammals: Time and food. J. Biol. Rhythms 18, 250–260 (2003).
- I. G. Gould, P. Tsai, D. Kleinfeld, A. Linninger, The capillary bed offers the largest hemodynamic resistance to the cortical blood supply. J. Cereb. Blood Flow Metab. 37, 52–68 (2017).
- E. E. Abrahamson, R. Y. Moore, Suprachiasmatic nucleus in the mouse: Retinal innervation, intrinsic organization and efferent projections. *Brain Res.* 916, 172–191 (2001).
- H. C. Cormier, V. Della-Maggiore, I. N. Karatsoreos, M. M. Koletar, M. R. Ralph, Suprachiasmatic vasopressin and the circadian regulation of voluntary locomotor behavior. *Eur. J. Neurosci.* 41, 79–88 (2015).
- X. Jin, L. P. Shearman, D. R. Weaver, M. J. Zylka, G. J. de Vries, S. M. Reppert, A molecular mechanism regulating rhythmic output from the suprachiasmatic circadian clock. *Cell* 96, 57–68 (1999).
- R. Silver, A. I. Sookhoo, J. LeSauter, P. Stevens, H. T. Jansen, M. N. Lehman, Multiple regulatory elements result in regional specificity in circadian rhythms of neuropeptide expression in mouse SCN. *Neuroreport* 10, 3165–3174 (1999).
- M. Mieda, D. Ono, E. Hasegawa, H. Okamoto, K. Honma, S. Honma, T. Sakurai, Cellular clocks in AVP neurons of the SCN are critical for interneuronal coupling regulating circadian behavior rhythm. *Neuron* 85, 1103–1116 (2015).
- Y. Yamaguchi, T. Suzuki, Y. Mizoro, H. Kori, K. Okada, Y. Chen, J. M. Fustin, F. Yamazaki, N. Mizuguchi, J. Zhang, X. Dong, G. Tsujimoto, Y. Okuno, M. Doi, H. Okamura, Mice genetically deficient in vasopressin V1a and V1b receptors are resistant to jet lag. Science 342, 85–90 (2013).
- C. Gizowski, C. Zaelzer, C. W. Bourque, Clock-driven vasopressin neurotransmission mediates anticipatory thirst prior to sleep. *Nature* 537, 685–688 (2016).
- Y. Ueta, H. Fujihara, R. Serino, G. Dayanithi, H. Ozawa, K. Matsuda, M. Kawata, J. Yamada,
   Ueno, A. Fukuda, D. Murphy, Transgenic expression of enhanced green fluorescent protein enables direct visualization for physiological studies of vasopressin neurons and isolated nerve terminals of the rat. *Endocrinology* 146, 406–413 (2005).
- N. Renier, E. L. Adams, C. Kirst, Z. Wu, R. Azevedo, J. Kohl, A. E. Autry, L. Kadiri, K. Umadevi Venkataraju, Y. Zhou, V. X. Wang, C. Y. Tang, O. Olsen, C. Dulac, P. Osten, M. Tessier-Lavigne, Mapping of brain activity by automated volume analysis of immediate early genes. *Cell* 165, 1789–1802 (2016).
- M. Ludwig, G. Leng, Autoinhibition of supraoptic nucleus vasopressin neurons in vivo: A combined retrodialysis/electrophysiological study in rats. Eur. J. Neurosci. 9, 2532–2540 (1997).
- S. J. Son, J. A. Filosa, E. S. Potapenko, V. C. Biancardi, H. Zheng, K. P. Patel, V. A. Tobin, M. Ludwig, J. E. Stern, Dendritic peptide release mediates interpopulation crosstalk between neurosecretory and preautonomic networks. *Neuron* 78, 1036–1049 (2013).
- 38. G. Paxinos, C. Watson, *The Rat Brain in Stereotaxic Coordinates* (Academic Press, ed. 5, 2005).

**Acknowledgments:** We thank F. Althammer (GSU) for general technical assistance. We also thank N. Bolger (CU) for guidance with the Bayesian analysis. **Funding:** This work was supported by the American Heart Association, grant 916907 (to R.K.R.); NSF, grant 1749500 (to R.S.); and the Columbia University Zuckerman Institute's Cellular Imaging Platform, NIH 1S100D023587-01, NHLBI 090948, and NINDS 094640 (to J.E.S.); AHA, 953524 (to V.C.B.); and

### SCIENCE ADVANCES | RESEARCH ARTICLE

the Center for Neuroinflammation and Cardiometabolic Diseases at Georgia State University. **Author contributions:** R.K.R.: writing—original draft, conceptualization, investigation, writing—review and editing, methodology, validation, formal analysis, project administration, and visualization. Y.Y.: writing—original draft, conceptualization, investigation, writing—review and editing, methodology, validation, and visualization. I.K.G.: investigation, writing—review and editing, and visualization. A.V.A: methodology, resources, data curation, validation, formal analysis, and visualization. V.C.B.: writing—original draft, investigation, writing—review and editing, methodology, resources, data curation, validation, supervision, formal analysis, project administration, and visualization. R.S.: writing—original draft, conceptualization, investigation, writing—review and editing, methodology, resources, funding acquisition, data curation, validation, formal analysis,

project administration, and visualization. J.E.S.: writing—original draft, conceptualization, investigation, writing—review and editing, methodology, resources, funding acquisition, validation, supervision, formal analysis, project administration, and visualization.

Competing interests: The authors declare that they have no competing interests. Data and materials availability: All data needed to evaluate the conclusions in the paper are present in the paper and/or the Supplementary Materials. Source data are also provided with this paper.

Submitted 2 January 2024 Accepted 16 May 2024 Published 21 June 2024 10.1126/sciadv.adn8350